# Measurement of Beam-Spin Asymmetries for
# $\pi^+$ Electroproduction Above the Baryon Resonance Region

H. Avakian,[1,2] V.D. Burkert,[1] L. Elouadrhiri,[1] N. Bianchi,[2] G. Adams,[30] A. Afanasev,[1] P. Ambrozewicz,[12] E. Anciant,[4] M. Anghinolfi,[16] D.S. Armstrong,[37] B. Asavapibhop,[23] G. Audit,[4] T. Auger,[4] H. Bagdasaryan,[38] J.P. Ball,[3] S. Barrow,[13] M. Battaglieri,[16] K. Beard,[20] M. Bektasoglu,[26,21] M. Bellis,[30] N. Benmouna,[14] A.S. Biselli,[6,30] S. Boiarinov,[19,1] B.E. Bonner,[31] S. Bouchigny,[17,1] R. Bradford,[6] D. Branford,[11] W.K. Brooks,[1] C. Butuceanu,[37] J.R. Calarco,[24] D.S. Carman,[26] B. Carnahan,[7] C. Cetina,[14] L. Ciciani,[27] P.L. Cole,[34,1] A. Coleman,[37] D. Cords,[1] P. Corvisiero,[16] D. Crabb,[36] H. Crannell,[7] J.P. Cummings,[30] E. De Sanctis,[2] R. De Vita,[16] P.V. Degtyarenko,[1] H. Denizli,[28] L. Dennis,[13] K.V. Dharmawardane,[27] C. Djalali,[33] G.E. Dodge,[27] D. Doughty,[8,1] P. Dragovitsch,[13] M. Dugger,[3] S. Dytman,[28] O.P. Dzyubak,[33] M. Eckhause,[37] H. Egiyan,[1,37] K.S. Egiyan,[38] A. Empl,[30] P. Eugenio,[13] R. Fatemi,[36] R.J. Feuerbach,[6] J. Ficenec,[35] T.A. Forest,[27] H. Funsten,[37] S.J. Gaff,[10] G. Gavalian,[24,38] S. Gilad,[22] G.P. Gilfoyle,[32] K.L. Giovanetti,[20] P. Girard,[33] C.I.O. Gordon,[15] K. Griffioen,[37] M. Guidal,[17] M. Guillo,[33] L. Guo,[1] V. Gyurjyan,[1] C. Hadjidakis,[17] R.S. Hakobyan,[7] J. Hardie,[8,1] D. Heddle,[8,1] P. Heimberg,[14] F.W. Hersman,[24] K. Hicks,[26] R.S. Hicks,[23] M. Holtrop,[24] J. Hu,[30] C.E. Hyde-Wright,[27] Y. Ilieva,[14] M.M. Ito,[1] D. Jenkins,[35] K. Joo,[1,36] J.H. Kelley,[10] J. Kellie,[15] M. Khandaker,[25] D.H. Kim,[21] K.Y. Kim,[28] K. Kim,[21] M.S. Kim,[21] W. Kim,[21] A. Klein,[27] F.J. Klein,[1,7] A. Klimenko,[27] M. Klusman,[30] M. Kossov,[19] L.H. Kramer,[12,1] Y. Kuang,[37] V. Kubarovsky,[30] S.E. Kuhn,[27] J. Lachniet,[6] J.M. Laget,[4] D. Lawrence,[23] K. Livingston,[15] Ji Li,[30] A. Longhi,[7] K. Lukashin,[1,7] J.J. Manak,[1] C. Marchand,[4] S. McAleer,[13] J.W.C. McNabb,[6] B.A. Mecking,[1] S. Mehrabyan,[28] J.J. Melone,[15] M.D. Mestayer,[1] C.A. Meyer,[6] K. Mikhailov,[19] R. Minehart,[36] M. Mirazita,[2] R. Miskimen,[23] L. Morand,[4] S.A. Morrow,[4] V. Muccifora,[2] J. Mueller,[28] G.S. Mutchler,[31] J. Napolitano,[30] R. Nasseripour,[12] S.O. Nelson,[10] S. Niccolai,[14] G. Niculescu,[26] I. Niculescu,[20,14] B.B. Niczyporuk,[1] R.A. Niyazov,[27] M. Nozar,[1] G.V. O'Rielly,[14] A.K. Opper,[26] M. Osipenko,[16] K. Park,[21] E. Pasyuk,[3] G. Peterson,[23] N. Pivnyuk,[19] D. Pocanic,[36] O. Pogorelko,[19] E. Polli,[2] S. Pozdniakov,[19] B.M. Preedom,[33] J.W. Price,[5] Y. Prok,[36] D. Protopopescu,[24] L.M. Qin,[27] B.A. Raue,[12,1] G. Riccardi,[13] G. Ricco,[16] M. Ripani,[16] B.G. Ritchie,[3] F. Ronchetti,[2,29] P. Rossi,[2] D. Rowntree,[22] P.D. Rubin,[32] F. Sabatié,[4,27] K. Sabourov,[10] C. Salgado,[25] J.P. Santoro,[35,1] V. Sapunenko,[16] M. Sargsyan,[12,1] R.A. Schumacher,[6] V.S. Serov,[19] Y.G. Sharabian,[38,1] J. Shaw,[23] S. Simionatto,[14] A.V. Skabelin,[22] E.S. Smith,[1] L.C. Smith,[36] D.I. Sober,[7] M. Spraker,[10] A. Stavinsky,[19] S. Stepanyan,[27] P. Stoler,[30] I.I. Strakovsky,[14] S. Strauch,[14] M. Taiuti,[16] S. Taylor,[31] D.J. Tedeschi,[33] U. Thoma,[1] R. Thompson,[28] L. Todor,[6] C. Tur,[33] M. Ungaro,[30] M.F. Vineyard,[32] A.V. Vlassov,[19] K. Wang,[36] L.B. Weinstein,[27] H. Weller,[10] D.P. Weygand,[1] C.S. Whisnant,[33,20] E. Wolin,[1] M.H. Wood,[33] A. Yegneswaran,[1] J. Yun,[27] B. Zhang,[22] J. Zhao,[22] and Z. Zhou[22,8]

(The CLAS Collaboration)

[1] *Thomas Jefferson National Accelerator Facility, Newport News, Virginia 23606*
[2] *INFN, Laboratori Nazionali di Frascati, 00044 Frascati, Italy*
[3] *Arizona State University, Tempe, Arizona 85287-1504*
[4] *CEA-Saclay, Service de Physique Nucleaire, F91191 Gif-sur-Yvette, Cedex, France*
[5] *University of California at Los Angeles, Los Angeles, California 90095-1547*
[6] *Carnegie Mellon University, Pittsburgh, Pennsylvania 15213*
[7] *Catholic University of America, Washington, D.C. 20064*
[8] *Christopher Newport University, Newport News, Virginia 23606*
[9] *University of Connecticut, Storrs, Connecticut 06269*
[10] *Duke University, Durham, North Carolina 27708-0305*
[11] *Edinburgh University, Edinburgh EH9 3JZ, United Kingdom*
[12] *Florida International University, Miami, Florida 33199*
[13] *Florida State University, Tallahassee, Florida 32306*
[14] *The George Washington University, Washington, DC 20052*
[15] *University of Glasgow, Glasgow G12 8QQ, United Kingdom*
[16] *INFN, Sezione di Genova, 16146 Genova, Italy*
[17] *Institut de Physique Nucleaire ORSAY, Orsay, France*
[18] *Institute für Strahlen und Kernphysik, Universität Bonn, Germany*
[19] *Institute of Theoretical and Experimental Physics, Moscow, 117259, Russia*
[20] *James Madison University, Harrisonburg, Virginia 22807*
[21] *Kyungpook National University, Taegu 702-701, South Korea*
[22] *Massachusetts Institute of Technology, Cambridge, Massachusetts 02139-4307*
[23] *University of Massachusetts, Amherst, Massachusetts 01003*

We report the first evidence for a non-zero beam-spin azimuthal asymmetry in the electroproduction of positive pions in the deep-inelastic kinematic region. Data for the reaction $ep \rightarrow e'\pi^+ X$ have been obtained using a polarized electron beam of 4.3 GeV with the CEBAF Large Acceptance Spectrometer at the Thomas Jefferson National Accelerator Facility (JLab). The amplitude of the $\sin\phi$ modulation increases with the momentum of the pion relative to the virtual photon, $z$. In the range $z = 0.5$–$0.8$ the average amplitude is $0.038 \pm 0.005 \pm 0.003$ for a missing mass $M_X > 1.1$ GeV and $0.037 \pm 0.007 \pm 0.004$ for $M_X > 1.4$ GeV.

The origin of the spin of the proton has become a topic of considerable experimental and theoretical interest since the EMC [1] measurements implied that quark helicities account for only a small fraction of the nucleon spin. As a consequence, the study of the gluon polarization and the orbital angular momentum of partons have become of central interest. Single-Spin Asymmetries (SSAs), measured in hadronic reactions for decades [2, 3], have emerged as important observables to access transverse momentum distributions of partons and the orbital angular momentum of quarks in the nucleon.

In this paper we present the first measurement of a non-zero beam-spin asymmetry in the electroproduction of positive pions in deep-inelastic kinematic region. Recently measurements of target SSAs have been reported for pion production in semi-inclusive deep-inelastic scattering (SIDIS) by the HERMES collaboration [4, 5, 6] for longitudinally polarized targets, and by the SMC collaboration for a transversely polarized target [7]. Such SSAs require a correlation between the spin direction of a particle and the orientation of the production (or scattering) plane, and have been linked to the orbital angular momentum of partons in the nucleon [8, 9]. Two fundamental QCD mechanisms giving rise to single spin asymmetries were identified. First the Collins mechanism [10, 11, 12], where the asymmetry is generated in the fragmentation of transversely polarized quarks, and second the Sivers mechanism [13, 14, 15, 16, 17, 18, 19], where it arises due to final state interactions at the distribution function level. The interference of wavefunctions with different orbital angular momentum, which is required to generate the SSA [16, 17, 18, 19], also yields

the helicity-flip Generalized Parton Distribution (GPD) $E$ [8, 9] that enters Deeply Virtual Compton Scattering (DVCS) [20, 21] and the Pauli form factor $F_2$. The connection of SSAs and GPDs has also been discussed in terms of the transverse distribution of quarks in nucleons [22, 23].

Physical observables accessible in SSAs include novel distribution and fragmentation functions such as chiral-odd transversity distribution [24, 25], the *time-reversal odd* (T-odd) distribution [13, 14, 15, 16, 17, 18, 19] and the Collins [10] T-odd fragmentation functions.

In the partonic description of SIDIS, distribution and fragmentation functions depend on the scaling variables $x$ and $z$, respectively (see below for the definition). At fixed and moderate values of the four momentum transfer $Q^2$ and at large values of $x$ and $z$, the contribution of multi-parton correlations or higher twist effects increases, eventually leading to a breakdown of the partonic description. Model calculations indicate that SSAs are less sensitive to a number of higher order corrections than cross section measurements in both semi-inclusive [26] and in hard exclusive [27, 28] pion production. The measurement of spin asymmetries could therefore become a major tool for studying quark transverse momentum dependent distributions [10, 11, 12, 13, 19, 29] and GPDs[27, 28] in the $Q^2$ domain of a few GeV$^2$.

The beam-spin asymmetries in single-pion production are higher-twist by their nature [11, 30, 31] and are expected to increase at low $Q^2$. Although large beam-spin asymmetries have been observed in measurements of exclusive electroproduction of photons (DVCS) [32, 33], the only measurement of the beam-spin asymmetry in semi-

inclusive pion electroproduction was reported recently by the HERMES collaboration [4] at $\langle z \rangle \approx 0.4$. Within statistical uncertainties their value is consistent with zero.

The cross section for single pion production by longitudinally polarized leptons scattering from unpolarized protons may be written in terms of a set of response functions. The helicity ($\lambda_e$) dependent part ($\sigma_{LU}$) [11, 29] arises from the anti-symmetric part of the hadronic tensor:

$$\frac{d\sigma_{LU}}{dx dy\, dz d^2 P_\perp} \propto \lambda_e \sqrt{y^2 + \gamma^2} \sqrt{1 - y - \frac{1}{4}\gamma^2} \sin\phi \; \mathcal{H}'_{LT}. \quad (1)$$

The subscripts in $\sigma_{LU}$ specify the beam and target polarizations, respectively ($L$ stands for longitudinally polarized and $U$ for unpolarized). The azimuthal angle $\phi$ is defined by a triple product:

$$\sin\phi = \frac{[\vec{k}_1 \times \vec{k}_2] \cdot \vec{P}_\perp}{|\vec{k}_1 \times \vec{k}_2||\vec{P}_\perp|},$$

where $\vec{k}_1$ and $\vec{k}_2$ are the initial and final electron momenta, and $\vec{P}_\perp$ is the transverse momentum of the observed hadron with respect to the virtual photon $\vec{q}$. The structure function $\mathcal{H}'_{LT}$ arises due to the interference of the longitudinal and transverse photon contributions. The kinematic variables $x$, $y$, and $z$ are defined as: $x = Q^2/2(P_1 q)$, $y = (P_1 q)/(P_1 k_1)$, $z = (P_1 P)/(P_1 q)$, where $Q^2 = -q^2$, $q = k_1 - k_2$ is the 4-momentum of the virtual photon, $P_1$ and $P$ are the momenta of the target and the observed final-state hadron, and $\gamma^2 = 4M^2 x^2 y^2/Q^2$.

The beam-spin asymmetries in single-pion semi-inclusive leptoproduction were measured using a 4.3 GeV electron beam and the CEBAF Large Acceptance Spectrometer (CLAS) [34] at JLab. Scattering of longitudinally polarized electrons off a liquid-hydrogen target was studied over a wide kinematic region. The beam polarization, frequently measured with a Møller polarimeter, was on average $0.70 \pm 0.03$. Beam helicity was flipped every 30 msec to minimize the helicity correlated systematics. The scattered electrons and pions were detected in CLAS. Electron candidates were selected by a hardware trigger using a coincidence between the gas Cherenkov counters and the lead-scintillator electromagnetic calorimeters. Pions in a momentum range of 1.2 to 2.6 GeV were identified using momentum reconstruction in the tracking system and the time-of-flight from the target to the timing scintillators. The total number of electron-$\pi^+$ coincidences in the DIS range ($Q^2 > 1$ GeV$^2$, $W^2 > 4$ GeV$^2$) was $\approx 4 \times 10^5$.

A critical issue in SIDIS processes is the assumption of factorization, i.e. that the hadron production cross section can be evaluated as a convolution of a $x$-dependent distribution function, a hard scattering and a $z$-dependent fragmentation function. This picture is
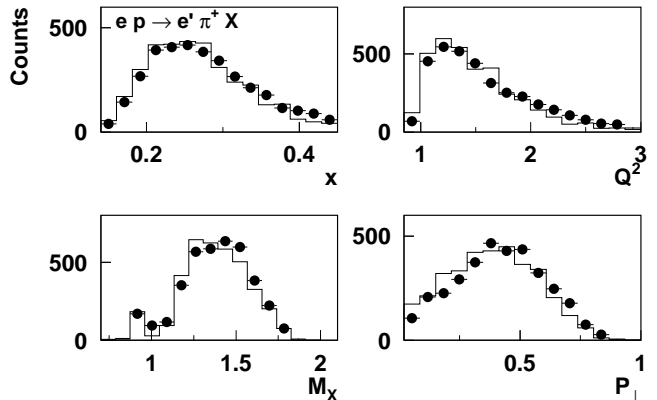


FIG. 1: Comparison of the distributions measured with CLAS at 4.3 GeV (circles) in $x, Q^2$(GeV$^2$), missing mass $M_X$(GeV), and the transverse pion momentum $P_\perp$(GeV) with LUND-MC reconstructed events. The distributions are averages over the range $0.5 < z < 0.8$; the MC results are normalized to the same number of events.

valid if the hadron originates from the fragmentation of the *current* quark, assuming there is sufficient energy so that the 4-momentum of the final hadron is not directly related to that of the struck quark. At low $z$ hadrons may additionally originate from the fragmentation of the target, while at large $z$, in addition to higher twist effects, diffractive effects are also important. Therefore a restricted range in $0.5 < z < 0.8$ has been selected for the analysis.

The event distributions in the restricted $z$-range have been compared with a Monte Carlo based on the LUND generator [35] developed to describe high energy processes. In LUND, the pion production is dominated by direct production from string fragmentation, as opposed to other processes such as target fragmentation and hadronic decays. Figure 1 shows comparisons between the experimental yields and the normalized MC distributions for different kinematical variables. The agreement of MC with the data suggests that the high energy-description of the SIDIS process can be extended to the moderate energies of this measurement.

To verify the factorization ansatz, pion multiplicities have been extracted for different $x$ ranges. Pion multiplicities have been shown to be approximately equivalent to fragmentation functions [36] which depend on the $z$ variable only at fixed $Q^2$. In Fig. 2 $\pi^+$ multiplicities normalized by the total number of events are shown as a function of $z$ for different $x$ bins. Within the range and the precision of the present measurement no $x$-dependence of multiplicities is seen. This experimental finding is also consistent with the assumption of factorization.
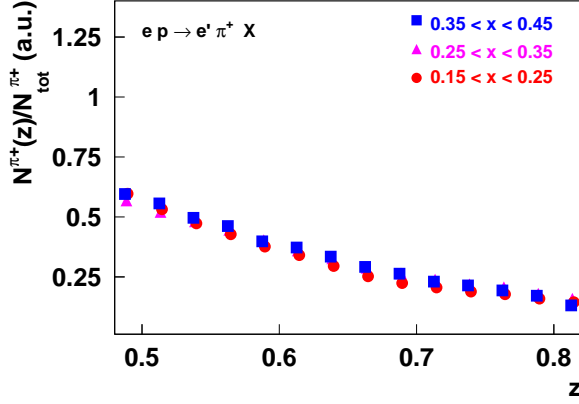
FIG. 2: Pion multiplicities as a function of $z$ for different $x$ ranges normalized by the total number of pions in the corresponding $x$-range.



FIG. 3: The beam-spin azimuthal asymmetry as a function of azimuthal angle $\phi$, measured in the range $z$=0.5–0.8.

The azimuthal distribution of the beam-spin asymmetry for $\pi^+$:

$$A(\phi)_{LU} = \frac{1}{P}\frac{N^+ - N^-}{N^+ + N^-}, \qquad (2)$$

is shown in Fig. 3. Here $N^{\pm}$ is the number of events for positive/negative helicities of the electron and $P$ is the beam polarization. The data show a clear $\sin\phi$ modulation from which a $\sin\phi$ moment of $0.038 \pm 0.005(stat)$ can be derived.

The same quantity can be formed by extracting moments of the cross section for the two helicity states weighted by the corresponding $\phi$-dependent functions. In this case the $\sin\phi$ moment is given by:

$$A_{LU}^{\sin\phi} = \frac{2}{PN^{\pm}}\sum_{i=1}^{N^{\pm}}\sin\phi_i, \qquad (3)$$

The two methods are identical for a full acceptance detector, but in practice have different sensitivities to acceptance effects. In Fig. 4 the comparison of $A_{LU}^{\sin\phi}$ derived with the two methods is presented as a function of the missing mass $M_X$ evaluated in the $ep \rightarrow e'\pi^+ X$ reaction. As can be seen the results agree well with each other over the full $M_X$ range. The moments $A_{LU}^{\sin\phi}$ can be also computed for each helicity state and for an average of zero helicity which corresponds to an unpolarized beam. These data shown in Fig. 4 provide an additional test of the absence of spurious azimuthal asymmetries. All these results indicate that within the statistical uncertainties, the acceptance corrections are small and under control.

Contributions to the systematic uncertainties arise from spin-dependent moments of the cross section coupling to corresponding moments in the acceptance to produce corrections to the measured $\sin\phi$ moment [4]. The
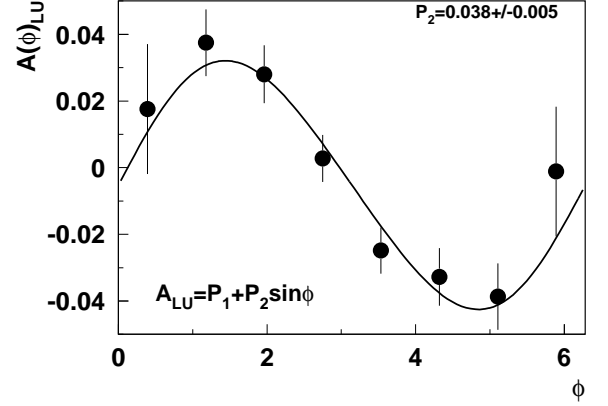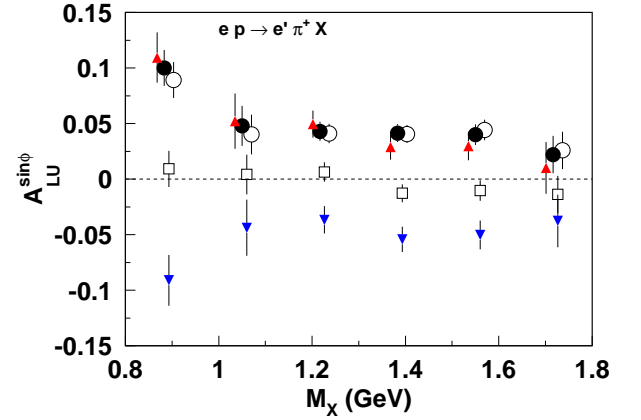


FIG. 4: The beam-spin azimuthal asymmetry as a function of missing mass $M_X$, in $\gamma^* p \rightarrow \pi^+ X$ extracted in the range $0.5 < z < 0.8$. Triangles up and down are the results for positive and negative helicities, respectively, and the filled circles are for their average. Open circles show the measured $A_{LU}^{\sin\phi}$ extracted as a $\sin\phi$ moment of the spin asymmetry. Open squares show the measured $A_{LU}^{\sin\phi}$ for the sample averaged over the beam polarization. Data are slightly shifted in $M_X$ for clarity.

contribution to uncertainties due to the CLAS acceptance in all relevant kinematic variables $(x, y, z, P_\perp, \phi)$ is evaluated to be less than 0.004 in average and less than 0.007 in all bins. The systematic uncertainties in the measurement of the beam polarization contribute at an even lower level (0.002). Possible particle misidentification over the accessible kinematic range changes the observed SSA by less than 0.001. To minimize radiative corrections, a cut on the energy of the virtual photon relative to the incoming electron ($y < 0.85$) was imposed.

The estimated radiative corrections do not exceed a few percent of the value of the SSA [37], and give a minor contribution to the systematic uncertainty. Other systematic uncertainties are negligible.

As can be seen in Fig. 4, the missing mass on the remnant system is mostly occurring in the nucleon resonance region. Despite this, the beam SSA doesn't show a dependence on any specific final state. A sizable increase of the SSA only appears in exclusive $\pi^+$ production where the missing mass corresponds to the nucleon mass. For this reason, two different cuts on the missing mass $M_X$ have been applied in the final analysis. A first cut at $M_X > 1.1$ GeV was chosen to exclude the contribution of the exclusive $\pi^+$ production on the nucleon. A higher cut at $M_X > 1.4$ GeV was also considered to reduce, in addition, the contribution of semi-exclusive $\pi^+$ production with a recoiling $\Delta^0$-resonance. For $M_X > 1.4$ GeV multi-hadron production is the dominant mechanism and the possible contribution of higher nucleon resonances in the recoiling system can be interpreted in terms of quark-hadron duality. This seems to be supported by the smooth and almost flat behavior of the data shown in Fig. 4.

A further check is shown in Fig. 5, where the $z$-dependence of the beam SSA is presented for increasing values of the missing mass cut. Due to the large correlation between the $z$ and the $M_X$ variables, an increasing $M_X$ cut drastically reduces the number of events with large $z$, leaving almost unchanged the beam SSA. This indicates that, within the present statistical uncertainties, the fraction $z$ of the virtual photon energy carried by the pion, rather than the missing mass $M_X$, is the relevant variable in the scattering process.

Consistency with the factorization assumption, which has been already shown in Fig. 2 for $\pi^+$ multiplicities, has also been investigated for the observable under study. In Fig. 6 the beam SSA is presented as a function of $z$ for different $x$-bins. Its general behavior suggested by the curve does not exhibit any significant $x$-dependence, which is also consistent with factorization in the chosen kinematic range.

The dependence of beam SSA on the $\pi^+$ transverse momentum, $P_\perp$, is shown in Fig. 7. A linear dependence of SSA on the $P_\perp$ (with kinematic zero at $P_\perp = 0$ GeV) is expected, at least for the moderate range of $P_\perp$ [11, 12].

The beam spin asymmetries averaged over the two spin states as a function of $x$ and $z$ are plotted in Fig. 8 and listed in Table I. Table II shows the relevant variables for the different $x$ and $z$ bins. The beam SSA is positive for a positive electron helicity over the entire measured range. The data do not show a significant $x$-dependence while the asymmetry is strongly increasing at high $z$, where according to LUND MC, the probability of the detected pion to carry the struck quark is maximal.

The size and the behavior of the asymmetry are very similar for the two cases of missing mass cuts. For the
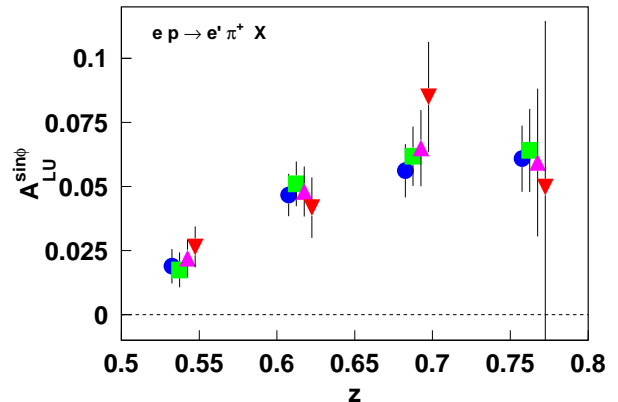


FIG. 5: The beam-spin azimuthal asymmetry as a function of $z$ extracted for different cuts on the missing mass $M_X$ (in GeV), $M_X > 1.1$ (circles), $M_X > 1.2$ (squares), $M_X > 1.3$ (triangles up) and $M_X > 1.4$ (triangles down).
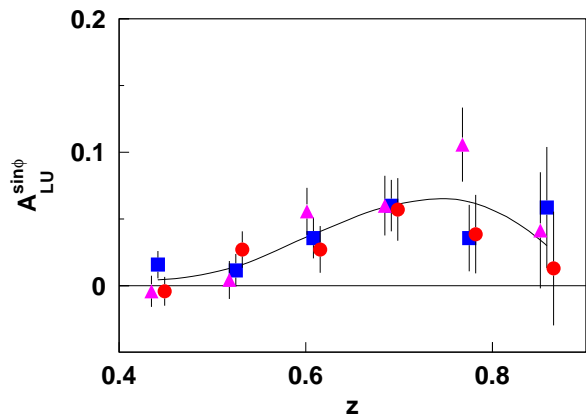


FIG. 6: Beam SSA as a function of $z$ for different $x$ ranges (same as in Fig. 2) for $M_X > 1.1$ GeV. The curve is a simple fit to all data to show the general behavior of the asymmetry.

case of higher $M_X$ cut, the data are compared with a prediction [31] based on the Sivers mechanism as the dynamical origin of the observable. Within this framework, the asymmetry is given by the convolution of the T-odd parton distribution $h_1^\perp$ with the twist-3 fragmentation function $E(x)$ [38, 39]. The latter function is responsible for the strong $z$-dependence of the asymmetry. Despite the fact that the formalism is much better suited for higher energy reactions, the agreement in size and behavior with the data is reasonable.

The CLAS preliminary data on the beam SSA have been also interpreted in terms of the Collins mechanism [29, 40, 41, 42] for a first determination of the twist-3
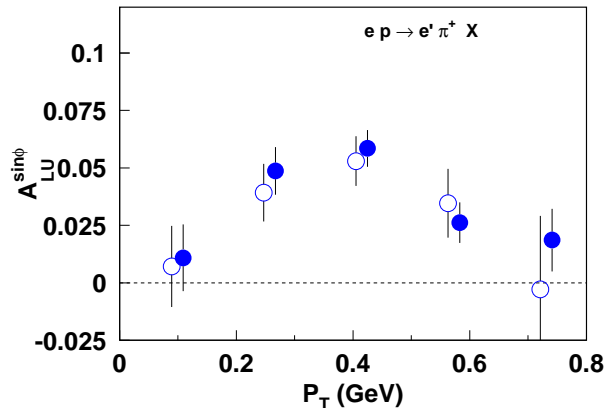
FIG. 7: Beam SSA as a function of $P_\perp$ for $M_X > 1.1$ GeV (filled circles) and $M_X > 1.4$ GeV (open circles).



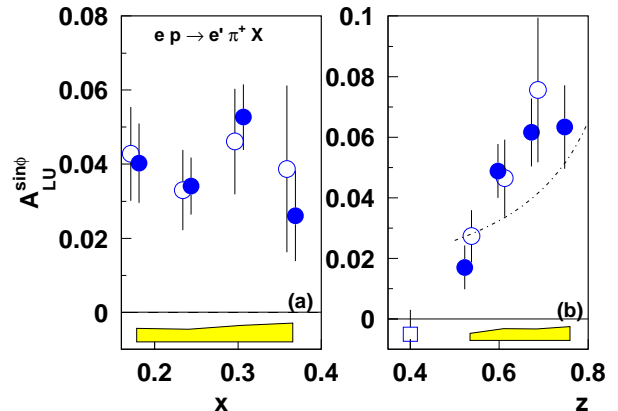FIG. 8: The beam-spin azimuthal asymmetry as a function of $x$ (a), in the range $0.5 < z < 0.8$, and as function of $z$ (b), in the range $0.15 < x < 0.4$ for $M_X > 1.1$ GeV (filled circles). The error bars show the statistical uncertainty, and the band represents the systematic uncertainties. The empty circles are results for $M_X > 1.4$ and have been slightly shifted to make them more visible. The empty square shows the HERMES result [4], which is an average over the range $z$=0.2–0.7 and $x$=0.02–0.4. The curve is a theoretical prediction [31].

distribution function $e(x)$ [40, 41]. The magnitude of their $e(x)$ is also consistent with predictions using the chiral quark soliton model [43, 44, 45].

At lower $z$ HERMES reported results consistent with zero beam-spin asymmetry [4]. CLAS asymmetries, obtained at higher $z$ and lower $Q^2$, should be kinematically enhanced with respect to the higher energy HERMES data [4], as pointed out in Refs. [30, 31], so that no evident contradiction can be inferred between the two measurements.

The data at lower $M_X$ demonstrate that for this observable the transition from the semi-inclusive to the semi-exclusive and to the exclusive domains is smooth. In addition these data may provide a new field for testing, in the final state, the quark-hadron duality, which has been proved to work in the initial state for other observables, like the spin-independent [46] and the spin-dependent [47] structure functions, down to low values of $Q^2$.

In conclusion, we have presented the first measurement of a non-zero beam-spin asymmetry in single $\pi^+$ inclusive electroproduction in the DIS kinematic region. The average asymmetry is $0.038 \pm 0.005 \pm 0.003$ for a missing mass $M_X > 1.1$ GeV and $0.037 \pm 0.007 \pm 0.004$ for $M_X > 1.4$ GeV. The asymmetry shows a strong enhancement at large values of $z$ while no significant $x$-dependence is present within the measured range. Detailed experimental and Monte Carlo studies have been performed showing no large violation of the factorization assumption for the process and suggesting that the partonic description may be applied in the kinematical range of the measurement. New data are expected from experiments utilizing a 6 GeV polarized beam, allowing a more precise test of the factorization ansatz and the investigation of the $Q^2$ dependence of the asymmetries.

[1] J. Ashman *et al.*, Phys. Lett. B **206**, 364 (1988).
[2] K. Heller *et al.*, Proceedings of Spin 96, Amsterdam, World Scientific Press, eds. C.W. de Jager *et al.* (1996).
[3] A. Bravar *et al.*, Phys. Rev. Lett. **77**, 2626 (1996).
[4] A. Airapetian *et al.*, Phys. Rev. Lett. **84**, 4047 (2000).
[5] A. Airapetian *et al.*, Phys. Rev. D **64**, 097101 (2001).
[6] A. Airapetian *et al.*, Phys. Lett. B **562**, 182 (2003).
[7] A. Bravar, Nucl. Phys. (Proc. Suppl.) B **79**, 521 (1999).
[8] S. Brodsky *et al.*, Nucl. Phys. B **642**, 344 (2002).
[9] X. Ji, J.-P. Ma, and F. Yuan, Nucl. Phys. B **652**, 383 (2003).
[10] J. Collins, Nucl. Phys. B **396**, 161 (1993).

[11] P. Mulders and R.D. Tangerman, Nucl. Phys. **B 461**, 197 (1996).
[12] A. Kotzinian, Nucl. Phys. **B 441**, 234 (1995).
[13] D. Sivers, Phys. Rev. D **43**, 261 (1991).
[14] M. Anselmino and F. Murgia, Phys. Lett. B **442**, 470 (1998).
[15] D. Boer and P. Mulders, Nucl. Phys. **B 569**, 505 (2000).
[16] S. Brodsky *et al.*, Phys. Lett. B **530**, 99 (2002).
[17] J. Collins, Phys. Lett. B **536**, 43 (2002).
[18] X. Ji and F. Yuan, Phys. Lett. B **543**, 66 (2002).
[19] A. Belitsky, X. Ji, and F. Yuan, Nucl. Phys. **B 656**, 165 (2003).
[20] X. Ji, Phys. Rev. Lett. **78**, 610 (1997).
[21] A.V. Radyushkin, Phys. Lett. B **380**, 417 (1996).
[22] M. Burkardt, Phys. Rev. D **66**, 114005 (2002).
[23] M. Burkardt and D.S. Hwang, e-Print Archive: hep-ph/0309072 (2003).
[24] J. Ralston and D. Soper, Nucl. Phys. **B 152**, 109 (1979)
[25] R.L. Jaffe and X. Ji, Nucl. Phys. **B 375**, 527 (1992).
[26] A. Bacchetta *et al.*, Phys. Rev. D **65**, 094021 (1999).
[27] L.L. Frankfurt *et al.*, Phys. Rev. D **60**, 014010 (1999).
[28] A. Belitsky and D. Muller, Phys. Lett. **B 513**, 349 (2001).
[29] J. Levelt and P. Mulders, Phys. Lett. B **338**, 357 (1994).
[30] A. Afanasev and C. Carlson, e-Print Archive: hep-ph/0308163 (2003).
[31] F. Yuan, e-Print Archive: hep-ph/0310279 (2003).
[32] A. Airapetian *et al.*, Phys. Rev. Lett. **87**, 182001 (2001).
[33] S. Stepanyan *et al.*, Phys. Rev. Lett. **87**, 182002 (2001).
[34] B. Mecking *et al.*, "The CLAS Detector", Nucl. Inst. & Meth. **503**, 513 (2003).
[35] L. Mankiewicz, A. Schafer, and M. Veltri, Comput. Phys. Commun. **71**, 305 (1992).
[36] A. Airapetian *et al.*, EPJ **C 21**, 599 (2001).
[37] A. Afanasev *et al.* Phys. Rev. D **66**, 074004 (2002).
[38] R.L. Jaffe and X. Ji, Phys. Rev. Lett. **71**, 2547 (1993).
[39] X. Ji, Phys. Rev. D **49**, 114 (1994).
[40] A. Efremov *et al.*, Nucl. Phys. **A711**, 84 (2002).
[41] A. Efremov *et al.*, Phys. Rev. D **67**, 114014 (2003).
[42] L. P. Gamberg, D. S. Hwang, and K. A. Oganessyan, hep-ph/0311221.
[43] P. Schweitzer, Phys. Rev. D **67**, 114010 (2003).
[44] M. Wakamatsu and Y. Ohnishi, Phys. Rev. D **67**, 114011 (2003).
[45] Y. Ohnishi and M. Wakamatsu, hep-ph/0311173.
[46] I. Niculescu *et al.*, Phys. Rev. Lett. **85**, 1186 (2000).
[47] A. Airapetian *et al.*, Phys. Rev. Lett. **90**, 092002 (2003).

TABLE I: SSA: $x$ and $z$-dependence for $M_X > 1.1$ GeV (upper table) and $M_X > 1.4$ GeV (lower table).

| $x$ | $A_{LU}^{\sin\phi} \pm \Delta_{stat} \pm \Delta_{syst}$ | $z$ | $A_{LU}^{\sin\phi} \pm \Delta_{stat} \pm \Delta_{syst}$ |
|---|---|---|---|
| 0.18 | $0.041 \pm 0.011 \pm 0.004$ | 0.54 | $0.017 \pm 0.007 \pm 0.002$ |
| 0.24 | $0.034 \pm 0.008 \pm 0.003$ | 0.61 | $0.049 \pm 0.009 \pm 0.004$ |
| 0.31 | $0.053 \pm 0.009 \pm 0.004$ | 0.69 | $0.062 \pm 0.011 \pm 0.004$ |
| 0.37 | $0.026 \pm 0.012 \pm 0.005$ | 0.76 | $0.063 \pm 0.014 \pm 0.005$ |
| 0.18 | $0.043 \pm 0.013 \pm 0.005$ | 0.54 | $0.027 \pm 0.009 \pm 0.003$ |
| 0.24 | $0.033 \pm 0.011 \pm 0.004$ | 0.61 | $0.047 \pm 0.013 \pm 0.005$ |
| 0.31 | $0.046 \pm 0.014 \pm 0.005$ | 0.69 | $0.076 \pm 0.024 \pm 0.005$ |
| 0.37 | $0.039 \pm 0.023 \pm 0.007$ | 0.76 | $0.067 \pm 0.080 \pm 0.007$ |

TABLE II: Average values of $Q^2$ (GeV$^2$), $W$ (GeV), $y$, $P_\perp$ (GeV) and $z/x$ in each of $x$ and $z$ bins for $M_X > 1.1$ GeV (upper table) and $M_X > 1.4$ GeV (lower table).

| $x$ | $\langle Q^2 \rangle$ | $\langle W \rangle$ | $\langle y \rangle$ | $\langle P_\perp \rangle$ | $\langle z \rangle$ | $z$ | $\langle Q^2 \rangle$ | $\langle W \rangle$ | $\langle P_\perp \rangle$ | $\langle x \rangle$ |
|---|---|---|---|---|---|---|---|---|---|---|
| 0.18 | 1.1 | 2.5 | 0.75 | 0.46 | 0.61 | 0.54 | 1.46 | 2.3 | 0.43 | 0.27 |
| 0.24 | 1.3 | 2.3 | 0.67 | 0.42 | 0.61 | 0.61 | 1.44 | 2.3 | 0.43 | 0.27 |
| 0.31 | 1.6 | 2.2 | 0.66 | 0.41 | 0.61 | 0.69 | 1.44 | 2.3 | 0.42 | 0.27 |
| 0.37 | 2.0 | 2.2 | 0.67 | 0.39 | 0.61 | 0.77 | 1.43 | 2.3 | 0.36 | 0.27 |
| 0.18 | 1.1 | 2.5 | 0.76 | 0.43 | 0.58 | 0.54 | 1.44 | 2.3 | 0.38 | 0.26 |
| 0.24 | 1.4 | 2.3 | 0.70 | 0.36 | 0.57 | 0.61 | 1.41 | 2.4 | 0.34 | 0.25 |
| 0.31 | 1.7 | 2.3 | 0.69 | 0.32 | 0.56 | 0.69 | 1.37 | 2.4 | 0.30 | 0.23 |
| 0.37 | 2.0 | 2.2 | 0.70 | 0.28 | 0.56 | 0.77 | 1.26 | 2.5 | 0.24 | 0.20 |